Polymer 51 (2010) 5649–5662

Contents lists available at ScienceDirect

Polymer

journal homepage: www.elsevier.com/locate/polymer

Feature Article

Proton binding by linear, branched, and hyperbranched polyelectrolytes

Ger J.M. Koper [a,*], Michal Borkovec [b]

[a] Department of Chemical Engineering, Delft University of Technology, Julianalaan 136, 2628 BL Delft, The Netherlands
[b] Department of Inorganic, Analytical, and Applied Chemistry, University of Geneva, Sciences II, 30, Quai Ernest-Ansermet, 1205 Geneva, Switzerland

ARTICLE INFO

Article history:
Received 22 June 2010
Received in revised form
23 August 2010
Accepted 27 August 2010
Available online 7 October 2010

Keywords:
Proton binding
Weak polyelectrolytes
Conformation

ABSTRACT

This article reviews our understanding of ionization processes of weak polyelectrolytes. The emphasis is put on a general introduction to site binding models, which are able to account for many experimental features of linear and branched polyelectrolytes, including dendrimers. These models are fully compatible with the classical description of acid–base equilibria. The review further discusses the nature of the site–site interaction and role of conformational equilibria. Experimental charging data of numerous weak polyelectrolytes are discussed in terms of these models in detail.

1. Introduction

The treatment of acids and bases represents an essential part of every chemistry program. Surprisingly, however, acid–base properties of polyelectrolytes are hardly discussed, even within an advanced polymer chemistry curriculum [1,2]. This disparity is largely related to the historical developments of the respective fields. While many aspects of acid–base equilibria of small molecules were clarified around the turn of the last century, only recently, we have started to understand physical–chemical properties of polyelectrolytes, including their acid–base behavior. Furthermore, the fundamental properties of polyelectrolytes are principally studied by polymer physicists, and this community is less inclined to address typically chemical aspects, such as, their acid–base properties. Recently, however, reviews addressing this subject have appeared [3–6].

The classical distinction between strong and weak polyelectrolytes is related to their proton binding affinity. In analogy to strong acids and bases, strong polyelectrolytes are fully ionized and their charge is basically independent of solution pH. Weak polyelectrolytes are only partially ionized, and their charge varies with solution pH due to binding of protons, alike to classical weak acids or bases. However, the proton binding isotherms (or charging curves) of weak polyelectrolytes are non-trivial, and normally cannot be described with the equilibrium models that have been developed to describe weak oligomeric acids or bases with few ionizable groups.

In most weak polyelectrolytes, one encounters two main types of ionizable groups. Weak polyacids normally feature carboxylic groups

$$R-COO^- + H^+ \rightleftharpoons R-COOH$$

whereby the deprotonated state is negatively charged and the protonated state is neutral. Weak polybases often contain primary amine groups

$$R-NH_2 + H^+ \rightleftharpoons R-NH_3^+$$

The deprotonated state is neutral and the protonated state positively charged. Secondary and tertiary amines behave similarly.

Classical theories of acid–base reactions involving two or more protonation steps tacitly invoke macroscopic chemical equilibria. Macroscopic species entering such equilibria are fictitious species defined by the total number of protons bound, and they provide no information, which groups are actually ionized and which ones are not. The corresponding macroscopic constants refer to the entire molecule and they cannot be normally assigned to single ionizable group. To circumvent this problem, some researchers introduce microscopic chemical equilibria [3,7–11]. Each microscopic species uniquely defines the protonation state of the molecule, which means that the ionization state of each individual group is specified. Microscopic equilibrium constants thus refer to the ionization reactions involving individual groups. The notion of microscopic equilibria is essential to address ionization behavior of weak polyelectrolytes, and therefore it will also be briefly discussed in the present review.

* Corresponding author.
E-mail address: g.j.m.koper@tudelft.nl (G.J.M. Koper).

0032-3861/$ – see front matter © 2010 Elsevier Ltd. All rights reserved.
doi:10.1016/j.polymer.2010.08.067

The fundamental concepts necessary for the understanding of acid–base equilibria of weak polyelectrolytes were laid down about fifty years ago by Steiner [12], Katchalsky et al. [13], and Marcus [14]. These scientists have recognized the important analogy between the ionization of a linear polyelectrolyte and a one-dimensional model of a magnet, which is normally referred to as the Ising model [15]. Many properties of the latter model were known at that time, as studies of magnets were always popular in the statistical mechanics community. When this model is applied to describe the ionization of a weak polyelectrolyte, it will be referred to as the site binding (SB) model. This model identifies interactions between the ionizable sites as essential model parameters, and thereby provides a fundamental framework to rationalize ionization properties of weak polyelectrolytes. In such systems, these interactions are mostly repulsive. In the context of magnets, repulsive interactions are referred to as anti-ferromagnetic, while biochemists call them non-cooperative interactions. Conversely, attractive interactions are referred to as ferromagnetic or cooperative [16–18]. Some authors have employed other terms used to describe magnets for polyelectrolytes. Strong polyelectrolytes are sometimes referred to as quenched and weak ones as annealed [5,19,20].

For weak site–site interactions, the corresponding SB model explains the characteristic broadening of the titration curve of weakly charged polyelectrolytes with respect to the one of the corresponding monoprotic acid or base as observed for poly(acrylic acid) (PAA) [21–25] or hyaluronic acid [26]. For stronger site–site interactions, the model further rationalizes the two distinct titration steps observed for highly charged polyelectrolytes, such as poly(fumaric acid) (PFA) [27], linear poly(ethylene imine) (LPEI) [28], or poly(vinyl amine) (PVA) [13]. The respective polycarboxylic acids are shown in Fig. 1. The mutual arrangement of the side groups, the so-called racemic structure, is highly relevant in these polyelectrolytes. More recently, variants of the SB model were put forward to explain the titration behavior of branched or star-like polyelectrolytes [20,29–34]. These models have been successfully used to rationalize the proton binding to branched and hyperbranched polyamines, see Fig. 2.

While research on acid–base properties of weak polyelectrolytes is ongoing in numerous groups, several aspects have only been addressed recently [4,5,20,35–48]. Let us mention the two most important topics here, namely the range of the site–site interactions [40,41,43] and the role of conformational degrees of freedom [35–37].

First, the site–site interactions entering the site binding models must be sufficiently short ranged in order to reproduce the detailed features of the experimental titration curves observed in polyelectrolytes. Long-ranged site–site interactions lead to broad and featureless titration curves, which are often at odds with the experiment. On the other hand, these interactions are dictated by electrostatic Coulomb interactions between the ionized sites. This seeming contradiction between the long-range character of Coulomb interactions and the short-ranged nature of the site–site interactions as inferred from titration experiments is poorly understood, and could be related to the important drop in the dielectric permittivity from the polymer backbone and the aqueous solution [40,41,43]. This mechanism will be discussed in more detail below. Based on this picture, one can further obtain a better understanding of the smearing-out mean-field approximations based on the Debye–Hückel (DH) and Poisson–Boltzmann (PB) models [3,22,27]. However, such models can be only justified for weakly charged systems.

Second, the ionization of weak polyelectrolytes is often accompanied by conformational transitions [35]. In some cases, conformational changes are simply dictated from the buildup of the line charge, and often they lead to a more extended conformation at higher charge densities. These degrees of freedom may further induce higher order interactions between the sites, most notably involving three sites (i.e., triplet interactions). In other cases, the ionization of the polyelectrolyte and its conformation are strongly coupled. In the latter situation, one may observe sudden transitions in the polyelectrolyte conformation and charge, which resemble first-order phase transitions [35–37,49–51]. Detailed studies of conformational transitions in hyperbranched polymers have been initiated recently [52–54].

Affinity distributions have also been used to describe the broadening of the binding isotherm in polyelectrolytes [55–59]. This approach describes the isotherm with a set of fictitious non-interacting sites, which have the same binding isotherm as the polyelectrolyte in question. In some cases, the exact distributions

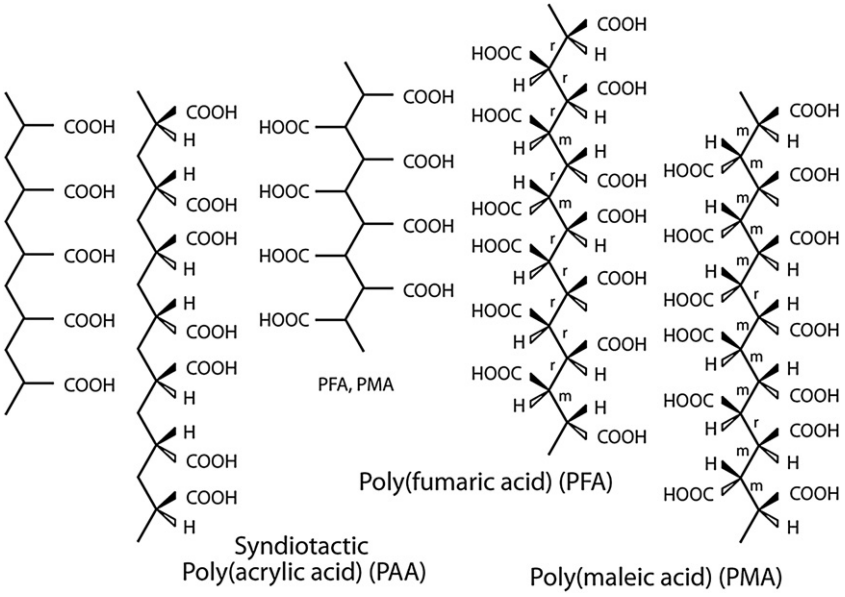

Fig. 1. Chemical and stereochemical structures of various polycarboxylic acids. PAA is often syndiotactic. In PMA every second bond is racemic and about 1/3 from the remaining ones are mesomeric, while in PFA every second bond is mesomeric (m) and about 1/2 from the remaining ones are racemic (r).

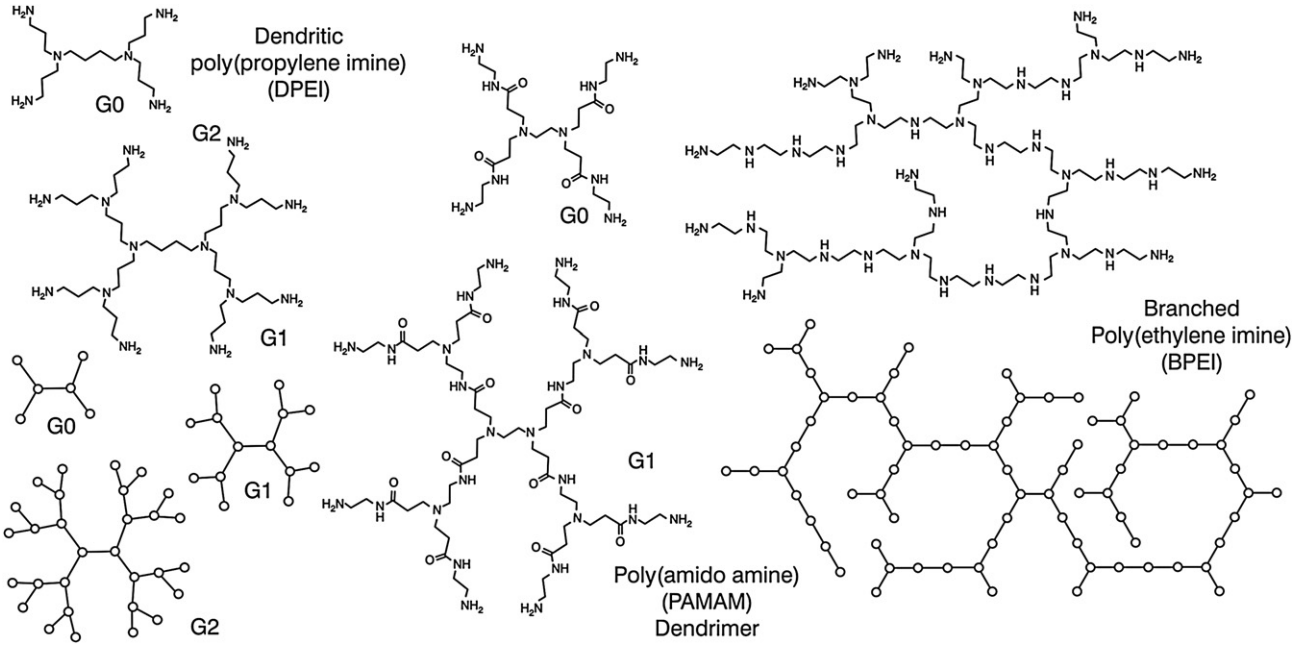

Fig. 2. Chemical structures with schematic representations of various branched polyamines. Dendritic poly(propylene imine) (PPI) and poly(amido amine) (PAMAM) dendrimers of different generations (left) and a possible structure of randomly branched poly(ethylene imine) (BPEI, right).

can be found for models with identical but interacting sites [55–58]. This approach provides less insight into systems where site–site interactions are important, but is much more useful to parameterize heterogeneous systems, such as humic acids [57–59].

The present review discusses the current state of understanding of the acid–base properties of weak polyelectrolytes. The aim is to provide an introduction to the field for the non-specialist and to make close contact with experiment. The review will first address the SB models and illustrate their basic features with simple examples. Subsequently, the effects of the range of the interactions between the ionizable sites and conformational degrees of freedom will be discussed. Finally, these models will be used to rationalize the experimentally observed charging behavior in various polyelectrolyte systems. We will only address dilute polyelectrolyte solutions where an excess of an indifferent salt has been added. In this case, interactions between different polyelectrolyte chains can be neglected, and ionization properties can be understood based on the structure of an isolated polyelectrolyte chain.

2. Site binding models

The site binding (SB) model provides a straightforward way to understand the relation between the titration properties of small oligomeric acids or bases and weak polyelectrolytes [3,4,14,30,43]. This model considers the protonation state of each individual site, and represents a generalization of the microscopic description of acid–base equilibria [3,7–11]. For simplicity, consider ionizable sites to be arranged in an equidistant fashion along a straight line. These sites are numbered from the left to the right with an index i, which runs over all sites of the molecule $i = 1,2,\ldots,N$ where N is the total number of all ionizable sites. For a monoprotic, diprotic or triprotic acid or base one has $N = 1$, 2, and 3, respectively. For a polyelectrolyte, this number is large, typically a few hundred, and in this situation one can consider the limit $N \to \infty$.

To define the protonation state of each site, we introduce discrete state variables s_i such that $s_i = 1$ when the site i is protonated and $s_i = 0$ when it is deprotonated. The set of all variables $s_1,s_2,\ldots,s_N$ uniquely characterizes the protonation state of all sites in the molecule (i.e., microstate). The nearest-neighbor SB model assumes that the free energy of an ionizable molecule can be approximated by a quadratic expression in the state variables s_i, namely

$$\frac{\beta F(s_1, s_2, \ldots, s_N)}{\ln 10} = -\sum_i \mathrm{p}K_i s_i + \sum_{i>j} \varepsilon_{ij} s_i s_j \tag{1}$$

where $\mathrm{p}K_i$ is the microscopic constant of the site i, ε_{ij} is the pair interaction parameter between site i and site j, and the thermal energy is $1/\beta = kT$ where k is the Boltzmann constant, and T is the absolute temperature. The relevant information on the binding properties is contained in the semi-grand partition function

$$\Xi = \sum_{s_1,\ldots,s_N} a_{\mathrm{H}}^n e^{-\beta F(s_1,\ldots,s_N)} \tag{2}$$

where a_{H} is the activity of protons, $\mathrm{pH} = -\log a_{\mathrm{H}}$, and n the number of protons bound in the microstate considered, namely $n = \sum_{j=1}^{N} s_j$. The sum in eq. (2) runs over all possible values of $s_1 = 0,1$, $s_2 = 0,1$, …, $s_N = 0,1$. When grouping terms of the same power in the activity, one finds that this partition function is equivalent to the so-called binding polynomial [3,60]

$$\Xi = \sum_{n=0}^{N} \overline{K}_n a_{\mathrm{H}}^n \tag{3}$$

where the coefficients $\overline{K}_n$ are the formation constants related to the macroscopic binding constants by $\mathrm{p}\overline{K}_n = \log(\overline{K}_n/\overline{K}_{n-1})$ and $\overline{K}_0 = 1$. The proton binding isotherm is given by the derivative

$$\theta = \frac{a_{\mathrm{H}}}{N} \cdot \frac{\partial \ln \Xi}{\partial a_{\mathrm{H}}} \tag{4}$$

where θ is the degree of protonation. By taking similar derivatives, other quantities of interest can be obtained, such as, site-specific titration curves or heat of binding.

The microscopic constants for other protonation states follow directly from SB model as well [3,8–11]. These constants can be defined for each site i provided all other sites are in a well-defined protonation state. The latter can be characterized by the state variables $s_1,s_2,\ldots,s_N$, and microscopic constants can be expressed as [9]

$$\mathrm{p}K_i(s_1,\ldots,s_N) = \mathrm{p}K_i - \sum_{i\neq j}\varepsilon_{ij}s_j \tag{5}$$

Note that when all sites are deprotonated the microscopic constant $\mathrm{p}K_i$ introduced in eq. (1) is identical to the microscopic constant $\mathrm{p}K_i(0,\ldots,0)$ of the site i provided all other sites are deprotonated. Such microscopic constants will be useful for the discussion of the proton binding isotherms below.

For a small number of sites, these expressions can be evaluated by simple inspection, and they lead to the known formulas for the binding equilibria of oligomeric acids and bases. For a simple acid or base ($N=1$), the binding polynomial becomes

$$\Xi = 1 + Ka_{\mathrm{H}} \tag{6}$$

where K is the binding constant, which is normally reported as $\mathrm{p}K = \log K$. Note that when the dissociation constant instead of the binding constant is being used, a minus sign appears in front of the logarithm of the latter relation. In this case, the microscopic and macroscopic constants are identical. The resulting binding isotherm is the well-known Langmuir isotherm

$$\theta = \frac{Ka_{\mathrm{H}}}{1+Ka_{\mathrm{H}}} \tag{7}$$

and is shown for $\mathrm{p}K=10$ in Fig. 3 ($N=1$). In the semi-logarithmic representation, this curve has the characteristic sigmoid appearance. One also writes this isotherm in its logarithmic form which is associated with the names of Henderson and Hasselbalch

$$\mathrm{pH} = \mathrm{p}K + \log\frac{1-\theta}{\theta} \tag{8}$$

In the case of a diprotic acid or base ($N=2$) the binding polynomial becomes

$$\Xi = 1 + \overline{K}_1\, a_{\mathrm{H}} + \overline{K}_2\, a_{\mathrm{H}}^2 \tag{9}$$

From this expression, the proton binding isotherm of a diprotic acid or base follows as

$$\theta = \frac{1}{2}\cdot\frac{\overline{K}_1 a_{\mathrm{H}} + 2\overline{K}_2 a_{\mathrm{H}}^2}{1+\overline{K}_1 a_{\mathrm{H}} + \overline{K}_2 a_{\mathrm{H}}^2} \tag{10}$$

In the case of two identical sites, the macroscopic constants are given by

$$\begin{aligned}\mathrm{p}\overline{K}_1 &= \mathrm{p}K + \log 2\\ \mathrm{p}\overline{K}_2 &= \mathrm{p}K - \varepsilon - \log 2\end{aligned} \tag{11}$$

where ε is the pair interaction parameter, which characterizes the splitting between the macroscopic constants. This parameter was also introduced in the context of solution equilibria [3,8]. The corresponding microscopic constants are similar, but lack the combinatorial factor

$$\begin{aligned}\mathrm{p}K(0,0) &= \mathrm{p}K\\ \mathrm{p}K(0,1) &= \mathrm{p}K - \varepsilon\end{aligned} \tag{12}$$

The first constant corresponds to the protonation of the first site provided the second site is deprotonated, while the second constant refers to the second site provided the first one is protonated.

The corresponding isotherm is shown for $\mathrm{p}K=10$ and $\varepsilon=2$ in Fig. 3A ($N=2$). One observes two humps and an intermediate plateau, which are characteristic for a diprotic acid or base. Each protonation step can be identified with one hump, and their positions are given by the two microscopic constants. The first one corresponds the protonation of the first site with the corresponding microconstant $\mathrm{p}K=10$. The intermediate plateau at $\theta=1/2$ reflects the stability of the singly protonated species. The second hump corresponds to the protonation to the second site. Since the second site is already protonated, the corresponding microconstant is $\mathrm{p}K-\varepsilon=8$. The corresponding microstates are also shown in Fig. 3A.

A similar analysis can be carried out for larger linear oligoprotic acids or bases. The resulting titration curves are shown for $\mathrm{p}K=10$ and $\varepsilon=2$ in Fig. 3. Let us briefly discuss the case of the linear triprotic acid or base ($N=3$). Here, both the terminal groups protonate in basic conditions with the microconstant $\mathrm{p}K=10$. However, this doubly protonated microstate is highly stable, and

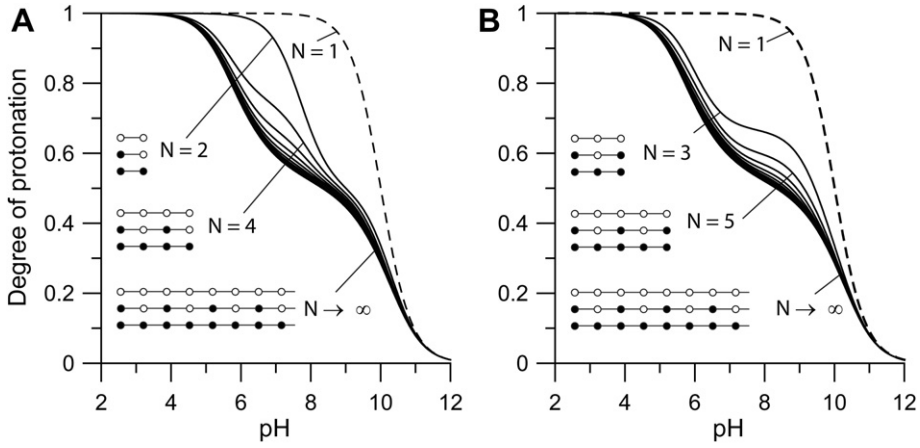

Fig. 3. Binding isotherms of linear oligomeric acids or bases for (A) even and (B) odd numbers of sites N and the corresponding polyelectrolyte ($N\to\infty$) calculated with the site binding model with identical sites. The model was evaluated for $\mathrm{p}K=10$ and nearest-neighbor interaction parameter $\varepsilon=2$. The succession from the deprotonated, partially protonated, and fully protonated states is indicated. The circles denote deprotonated (○) and protonated (●) sites. The alternating microstates are particularly stable and lead to intermediate plateaus.

leads to the intermediate plateau at $\theta = 1/3$. The last site protonates in more acidic conditions with a microconstant $pK - 2\varepsilon = 6$ since two pair interactions must be overcome.

With increasing chain length, the direct enumeration becomes increasingly tedious, and is impossible for the infinitely long chain. An elegant approach to evaluate the binding isotherm and the corresponding binding constants is the transfer matrix technique [61]. Let us briefly discuss this technique borrowed from statistical mechanics here. For a linear chain with nearest-neighbor pair interactions, the partition function can be written as

$$\Xi = \mathbf{s}^{\mathrm{T}}\mathbf{U}^{N}\mathbf{t} \tag{13}$$

We have introduced the transfer matrix

$$\mathbf{U} = \begin{bmatrix} 1 & z \\ 1 & zu \end{bmatrix} \tag{14}$$

where z is the reduced activity defined as $z = Ka_{\mathrm{H}}$ and $\varepsilon = -\log u$. The initiating row vector is $\mathbf{s}^{\mathrm{T}} = (1, 0)$ and the terminating column vector $\mathbf{t} = (1,1)^{\mathrm{T}}$ where the superscripted T denotes the transpose of a vector, which transforms a column vector into a row vector and vice versa.

This transfer matrix can be interpreted as follows. Both unit entries in the left column reflect the fact that the addition of one empty site to the chain does not change its free energy. Top right entry reflects the addition of a protonated site to the chain given the neighboring site is not protonated, and the corresponding contribution to the partition function is z. The bottom right entry corresponds to the addition of a protonated site given the neighboring site is protonated with a contribution zu to the partition function. In this case, the additional factor u accounts for the nearest-neighbor pair interaction.

One can verify that for small number of sites N, the transfer matrix expression eq. (13) reproduces all relations given above. However, the partition function can be also evaluated in the long chain limit ($N \to \infty$) analytically. In this limit, the partition function can be found from the largest eigenvalue of this transfer matrix $\mathbf{U}$ as [61]

$$\Xi \simeq \lambda^{N} \quad (N \to \infty) \tag{15}$$

where the eigenvalue is given by

$$\lambda = (1 + zu)/2 + \sqrt{z + (1 - uz)^2/4} \tag{16}$$

The binding isotherm follows from eq. (4) and one obtains

$$\theta = [2 + (\lambda/z)(1 - zu)/(1 - u + \lambda u)]^{-1} \tag{17}$$

The resulting titration curve is shown for $pK = 10$ and $\varepsilon = 2$ in Fig. 3 ($N \to \infty$). It features a characteristic plateau at half-protonation. One can understand the protonation mechanism as follows. In the basic region, the sites protonate initially independently with the microscopic constant $pK = 10$. This process continues until every second site is protonated. In this energetically favorable microstate, protonated and non-protonated sites alternate. This arrangement circumvents the unfavorable pair interactions, and leads to the intermediate plateau at $\theta = 1/2$. The remaining sites do protonate in the more acidic region. The corresponding protonation step occurs at $pK - 2\varepsilon = 6$ since two pair interactions must be overcome. The binding isotherm of the long chain resembles the one of a diprotic acid or base, but for the long chain the respective protonation steps are broader due to the existing disorder in the chain.

Fig. 3 demonstrates that the familiar binding curves for polyprotic acids and bases approach the liming case for the long chain relatively rapidly. One can further see that chains with odd or even number of sites converge differently to that limiting case. This difference can be again explained by the stability of the intermediate microstate with alternating protonated and deprotonated sites. For chains with odd number of sites, this microstate is unique, and leads to an intermediate plateau at $\theta = 1/2 + 1/(2N)$. For even number of sites, this intermediate state is not unique, and a clear intermediate plateau does not develop.

The present approach can be extended to branched structures in a straightforward way. The archetypal branched polyelectrolytes are the various types of polyamines depicted in Fig. 2. Other branched polyelectrolytes, such as complex polycarboxylates or humic acids will not be discussed here [58,59,62,63]. In contrast to the linear structures, which consist of doubly coordinated sites, the branched structures contain singly and triply coordinated sites. In the case of polyamines, the triply and singly coordinated sites correspond to primary and tertiary amines, while the doubly coordinated sites correspond to secondary amines. In the absence of rings, the numbers of triply and singly coordinates sites are the same for large polymers. The SB model can then be solved in various ways by generalizations of the transfer matrix technique or Monte Carlo simulation [29,30,64]. We will not discuss these technicalities here, but rather focus on the general picture.

There are two fundamentally different architectures of a branched polymer, namely the dendrimer and the comb, see Fig. 2. Whether the architecture of a branched polymer rather resembles a dendrimer or a comb can be quantified in terms of the compactness. Thereby, the dendrimer is the most compact structure, while the comb is the least compact one. Other structures can be thought of as intermediates between these two extremes. A branched polymer may equally contain doubly coordinated sites. This structural aspect can be quantified by the degree of branching, that is the fraction of triply coordinated sites. Most other branched structures can be thought of as combinations between these three extremes, namely the linear chain, the dendrimer, and the comb.

The protonation behavior of the linear chain within the simplest site binding model with nearest-neighbor pair interactions was discussed above and is shown in Fig. 3. The protonation behavior of the branched structures, namely the dendrimer and the comb, is illustrated for $pK = 10$ and $\varepsilon = 2$ in Fig. 4.

In analogy to a linear chain, the dendrimer also does protonate in two steps. However, the intermediate plateau lies at 2/3. This plateau corresponds to a stable microstate, where only the odd shells of the dendrimer are protonated. This microstate again avoids all nearest-neighbor pair interactions. The position of the two protonation steps can be rationalized as follows. In the basic region, every site protonates independently with a microscopic constant $pK = 10$. The system then passes through the intermediate plateau, and forms the stable structure where every non-protonated site is neighboring two protonated ones. Every non-protonated site has now three protonated neighbors, and subsequent protonation of these sites is determined by the microscopic constant $pK - 3\varepsilon = 4$. Thus, the two protonation steps are separated more widely for the dendrimer than for the corresponding linear chain.

The protonation behavior of the comb is more complicated, as it is characterized by two intermediate plateaus. In the basic region, every site will protonate independently with a microscopic constant $pK = 10$. When every second site becomes protonated, all pair interactions can be avoided by protonating the singly coordinated sites, which leads to an intermediate plateau at $\theta = 1/2$. The deprotonated sites on the backbone will have one neighboring site protonated, and in order to protonate they will have to overcome one pair interaction. This step will be characterized by the microscopic constant $pK - \varepsilon = 8$. The system protonates further until every second site of the backbone will be filled up. This configuration

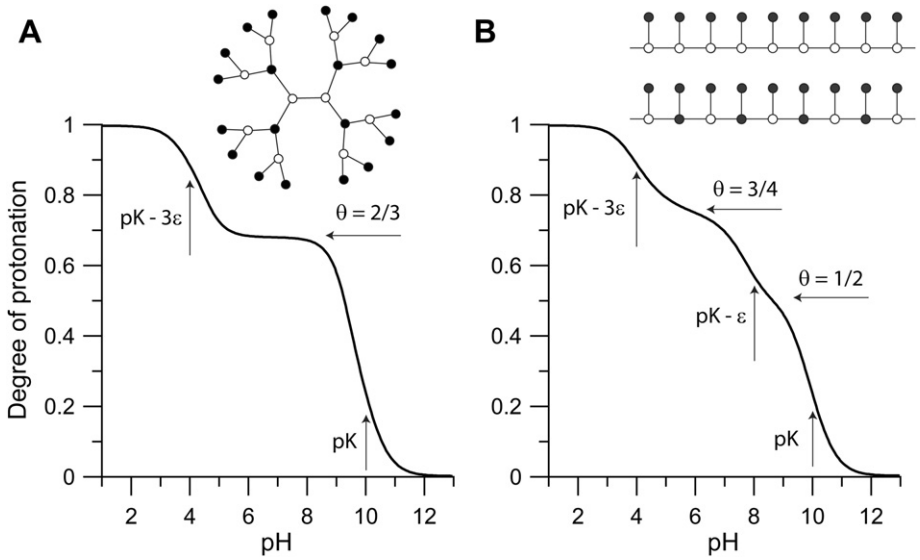

Fig. 4. Effect of branching on the titration of (A) dendritic and (B) comb-like weak polyelectrolytes. The site binding model with identical sites was evaluated for p$K = 10$ and nearest-neighbor interaction parameter $\varepsilon = 2$. The stable intermediate microstates are indicated as insets.

corresponds equally to a stable microstate, leading to a plateau at $\theta = 3/4$. Further protonation is possible only at sites, which have three neighboring sites that are protonated, and is therefore characterized by the microscopic constant p$K - 3\varepsilon = 4$. The stability of two different intermediate structures for the comb makes the titration curve smoother and more gradual.

This smoothening becomes even more prominent for other branched architectures, and represents an important characteristic of these systems. In the case of a randomly branched polyelectrolyte, the first half of the sites does protonate independently with a microscopic constant pK. The remaining deprotonated sites are not equivalent, as they have different environments. Some have one neighboring protonated site, others two, and some three. Further proton binding proceeds first through protonation of the sites with one protonated neighbor with a microscopic constant of p$K - \varepsilon$. Subsequently, the sites with two protonated neighbors protonate, with a constant of p$K - 2\varepsilon$. Finally, the remaining sites with three protonated neighbors protonate, and the corresponding constant is p$K - 3\varepsilon$. These different protonation steps will be rather closely spaced, and lead to a gradual increase of the binding isotherm.

Another reason for the smoothening of the binding isotherms for branched structures is that the binding constants of the differently coordinated sites are not the same due to their different chemical environments. For polyamines, the binding constants differ somewhat between the primary, secondary, and tertiary amines. These different groups protonate in different pH-regions, and broaden the binding isotherms further.

3. Range of site–site interactions

Repulsive interactions between the sites are primarily of electrostatic nature. For basic polyelectrolytes, such as polyamines, a protonated group is positively charged, while a deprotonated group is neutral. Two charged neighboring groups at a distance r will lead to a Coulombic energy contribution

$$W(r) = \frac{e^2}{4\pi\varepsilon_0 D_m}\cdot\frac{1}{r} \tag{18}$$

where e is the elementary charge, D_m is the (relative) dielectric constant of the medium, and ε_0 is the dielectric permittivity of vacuum. When an amine group protonates next to an already protonated site, the proton must overcome the repulsive Coulomb energy. The interaction parameter between the sites i and j entering in the free energy as defined in eq. (1) thus becomes

$$\varepsilon_{ij} = \frac{\beta W(r_{ij})}{\ln 10} \tag{19}$$

where r_{ij} is the distance between the respective sites. The interaction parameter turns out to be exactly the same for two acidic sites (e.g., carboxylic groups), which are negatively charged in the deprotonated state, or between basic and acidic sites. When groups of different charge are being considered, the interactions remain always repulsive, and any differences occur in the corresponding binding constants only. This situation arises since the protonation of an ionizable group always leads to an increase of its charge [3,41].

At larger distances, however, the presence of salt ions will weaken the electrostatic interactions and lead to screened Coulomb potential

$$W(r) = \frac{e^2}{4\pi\varepsilon_0 D_w}\cdot\frac{e^{-\kappa r}}{r} \tag{20}$$

where D_w is the dielectric constant of water and κ^{-1} is the Debye length defined by $\kappa^2 = 2kTe^2N_AI/(D_w\varepsilon_0)$ where I is the ionic strength and N_A the Avogadro's number. Therefore, site–site interactions will be negligible at distances substantially larger than the Debye length.

The pair interaction parameter of $\varepsilon = 2$ used in the preceding section corresponds in water to a distance between groups of 0.16 nm. This unrealistically small distance indicates that the relevant dielectric permittivity must be smaller than the one of water. This point is further illustrated by the fact that the characteristic two-step titration curve is never obtained when the screened Coulomb potential is used with a realistic set of parameters [40,41,43,64].

The dielectric environment within a carbon chain indeed has a lower dielectric permittivity than bulk water. This situation can be mimicked with a cylinder of a lower dielectric constant D_m that is immersed in a salt solution of a higher dielectric constant D_w [43]. Within this model, the ionizable sites are assumed to be arranged along the cylinder axis. The interaction between two such charged sites can be calculated explicitly, and the result is shown in Fig. 5. At

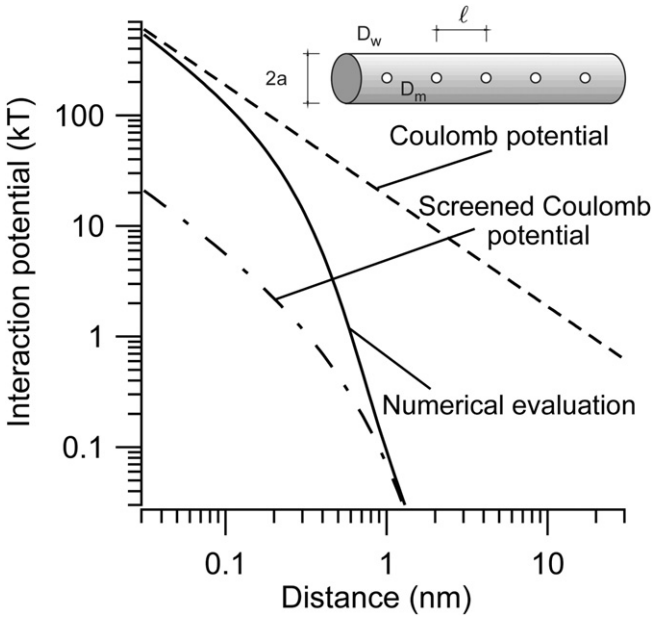

Fig. 5. Interaction potential between charged sites arranged along the axis of a cylinder of radius 0.25 nm and of a dielectric constant $D_m = 3$. The cylinder is immersed into an electrolytes solution with an ionic strength 0.5 M and a dielectric of $D_w = 80$ ($\kappa^{-1} = 0.43$ nm). The inset explains the parameters used.

small separation distances, the interaction potential is given by the Coulomb potential in a medium with the dielectric constant of the cylinder. At larger separation distances, the interaction potential follows the screened Coulomb potential in water with a higher dielectric constant. Since the interaction potential crosses over from one limiting law to the other, it decays very rapidly. This rapid decay is the likely reason why the consideration of nearest-neighbor interactions represents a good approximation for polyelectrolytes.

This interaction potential can be used to calculate the titration curve of a model polyelectrolyte with Monte Carlo simulations. The results of such a simulation, which take all interactions into account, are shown in Fig. 6A. One indeed observes the characteristic intermediate plateau and finds that the nearest-neighbor interaction model represents a good approximation. The data in Fig. 6B show the analogous situation for a polyelectrolyte with a lower charge density (i.e., larger spacing between the ionizable sites). In this case, the effect of interactions is weaker, and at the same time, the characteristic intermediate plateau disappears.

Let us now discuss another important simplification, which is useful to understand proton binding to weak polyelectrolytes, namely the mean-field approximation. Provided the interactions are not too strong, this approximation can be used to study SB models for large numbers of sites in a simple way. In that case, it is possible to replace the site variables by their average values, namely

$$s_i \to \langle s_i \rangle = \theta \tag{21}$$

With this approximation, one finds from eq. (1) that the strength of the mean-field is given by the mean-field interaction parameter

$$\bar{\varepsilon} = \frac{1}{N}\sum_{i \neq j} \varepsilon_{ij} \tag{22}$$

When the resulting free energy is minimized one obtains an isotherm, which in the present context is best written as

$$\mathrm{pH} = \mathrm{p}K_{\mathrm{eff}} + \log\frac{1-\theta}{\theta} \tag{23}$$

where

$$\mathrm{p}K_{\mathrm{eff}} = \mathrm{p}K - \bar{\varepsilon}\theta \tag{24}$$

Eq. (23) is very similar to eq. (8), but one has made the replacement $\mathrm{p}K \to \mathrm{p}K_{\mathrm{eff}}$. The effective constant $\mathrm{p}K_{\mathrm{eff}}$ now depends on the degree of protonation, and can be interpreted as the microscopic constant of a site at a given degree of protonation.

The predictions of the mean-field model are equally shown in Fig. 6. The model describes the isotherm for the more weakly charged system very well. However, this model fails for the highly charged system, and particularly it is unable to predict the intermediate plateau in the binding isotherm.

Numerous authors introduce tacitly an additional approximation by assuming that the charge is uniformly smeared out on the cylinder. In this case, the cylinder can be described with a uniform line charge density λ and a corresponding surface potential ψ_0. In this case, one can show that the effective constant $\mathrm{p}K_{\mathrm{eff}}$ can be written as [3,21,27]

$$\mathrm{p}K_{\mathrm{eff}} = \mathrm{p}K_{\mathrm{int}} - \beta e \psi_0 \tag{25}$$

where we have $\mathrm{p}K_{\mathrm{int}}$ introduced the intrinsic constant, which the microscopic constant of the site when all other sites are in their neutral state. For a polyamine, the intrinsic constant is equivalent to

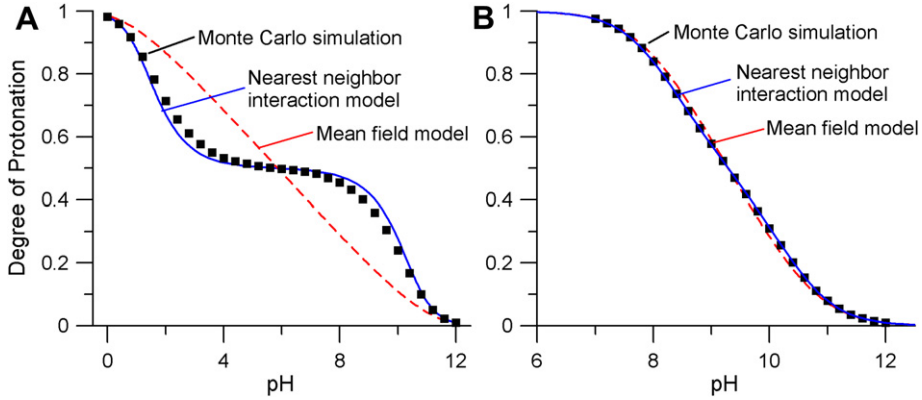

Fig. 6. Titration curves derived from discrete charge SB models for a linear polyelectrolyte. Comparison of Monte Carlo simulations (symbols), nearest-neighbor interaction model Eq. (17) and mean-field model Eq. (23). The dielectric constants are $D_m = 3$, $D_w = 80$ and the ionic strength 0.5 M ($\kappa^{-1} = 0.43$ nm). Ionizable sites are arranged along the axis of the cylinder of radius of 0.25 nm and have $\mathrm{p}K = 10$ and are uncharged in the deprotonated state. The spacing of the sites is (A) $\ell = 0.35$ nm and (B) $\ell = 0.55$ nm. The mean-field model represents a poor description for the polyelectrolyte with small spacing between the sites (A) while a good approximation for large spacing (B).

the microscopic constant introduced earlier when all sites are deprotonated. For a polycarboxylic acid, the intrinsic constant corresponds to the microscopic constant when all sites are protonated. To obtain a closed system of equations, one further needs the charge–potential relationship. For weakly charged systems, these two quantities are simply proportional [3]

$$\lambda = C\psi_0 \tag{26}$$

whereby the proportionality factor C is the capacitance per unit length. The line charge density can be related to the degree of protonation

$$\lambda = \frac{e}{\ell}(\theta - Z) \tag{27}$$

where ℓ is the distance between the groups along the chain and Z is the charge of the deprotonated group expressed in terms of the elementary charge e. Combining these equations, one obtains

$$\overline{\varepsilon} = \frac{\beta e^2}{C\ell \ln 10} \tag{28}$$

and

$$\mathrm{p}K = \mathrm{p}K_{\mathrm{int}} + Z\overline{\varepsilon} \tag{29}$$

Note that the charge of the group Z only enters the microscopic constant pK while the interaction parameter $\overline{\varepsilon}$ is independent of this quantity. To obtain an expression for the capacitance, one must invoke a detailed model of the charging behavior. The simplest model that can be used is the Debye–Hückel (DH) approximation, and one obtains a capacitance per unit length [65]

$$C = 2\pi\varepsilon_0 D_{\mathrm{w}} \kappa R \frac{K_1(\kappa R)}{K_0(\kappa R)} \tag{30}$$

where R is the cylinder of radius, and $K_n(x)$ is the modified Bessel function of the second kind of order n.

Fig. 7 illustrates the results from the DH cylinder model. The advantage of this model is that it also predicts a dependence on the ionic strength. This model suggests that the mean-field interaction parameter increases with decreasing ionic strength. The figure equally reflects the characteristic ionic strength dependence behavior expected for a polyamine and a polycarboxylate. In the latter case, the uncharged molecule is taken as the reference state and one assumes that the intrinsic constant pK_{int} does not depend on the ionic strength.

While the DH model predicts the correct trends with the ionic strengths, it normally overestimates these effects substantially. Extensions of this model have been considered by different authors. One important generalization is to use the Poisson–Boltzmann (PB) theory instead of the DH model, which yields a non-linear charge–potential relationship [3,21]. One may further introduce an additional Stern capacitance, which can be explained to originate

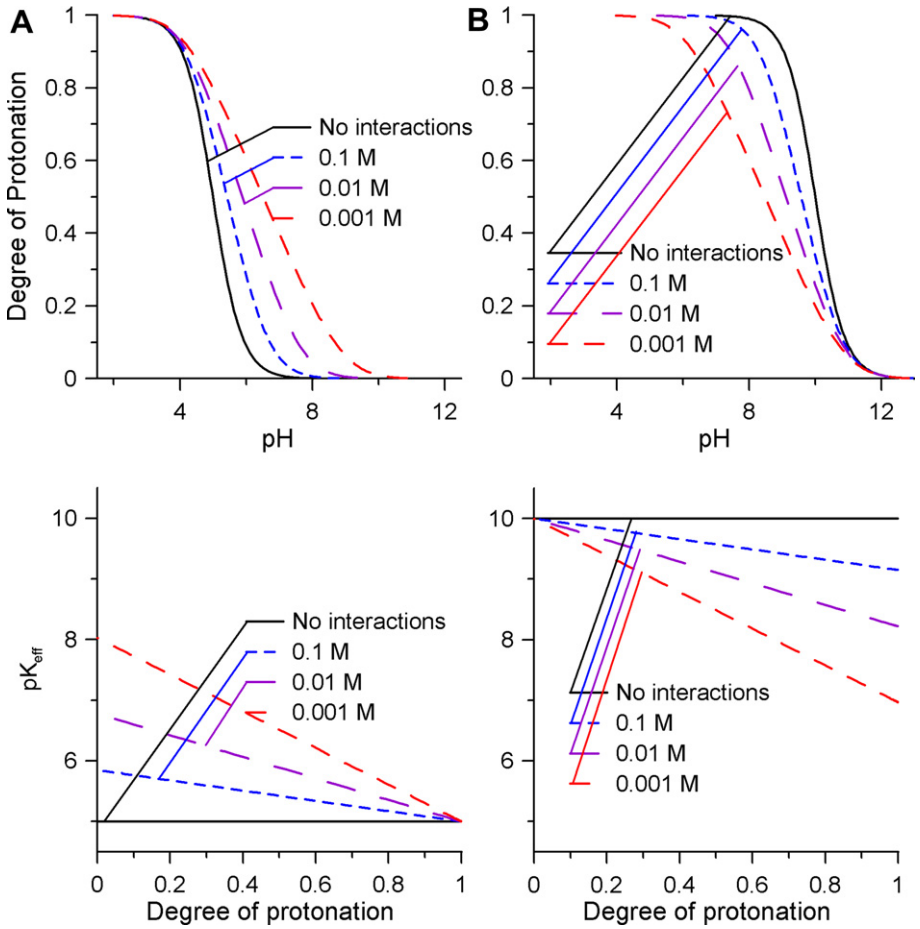

Fig. 7. Binding isotherms derived from the DH cylinder model for weak polyelectrolytes. The distance between the groups is 0.5 nm and the cylinder radius 1 nm. The model predictions are given for the ionic strengths of 0.001 (red line), 0.01 (purple line), and 0.1 M (blue line) leading to pair interaction parameters of $\overline{\varepsilon} = 3.03, 1.78$, and 0.85, respectively. The case of no interactions ($\overline{\varepsilon} = 0$) is shown as a black line for reference. Top row shows the degree of protonation θ as a function of pH and bottom row the effective binding constant pK_{eff} as a function of degree of protonation θ. (A) Polycarboxylate with p$K_{\mathrm{int}} = 5$and $Z = -1$ and (B) a polyamine with p$K_{\mathrm{int}} = 10$ and $Z = 0$. (For interpretation of the references to colour in this figure legend, the reader is referred to the web version of this article).

from the finite size of the counterions [25]. However, all these models are based on the smearing-out and mean-field approximations, which break down for highly charged systems. Moreover, PB theory will also fail for highly charged systems due to the neglect of ion correlations [4,39,66].

4. Conformational effects

Polyelectrolytes are not rigid, and their flexibility may substantially modify the interaction parameters entering the site binding model. Therefore, conformational changes influence the electrostatic interactions in between the ionized sites and thus modify the interactions in a polyelectrolyte chain.

Let us first discuss a simple model that captures the essence of the phenomenon. This model is based on the rotational isomeric state (RIS) model advocated by Flory [61]. In the simplest case of a symmetric chain, a bond can be in two different conformations, trans (t) and gauche (g). Assuming nearest-neighbor interactions only, the interactions within the chain can be also described by a 2×2 transfer matrix

$$\mathbf{V} = \begin{bmatrix} 1 & g \\ 1 & gh \end{bmatrix} \tag{31}$$

where g is the statistical weight of the gauche state and the parameter h defines the pair interaction between the gauche bonds. Based on this model, one can evaluate the probability of the various conformational states of the chain. Clearly, this model is entirely analogous to the SB model discussed above, see eq. (14).

The SB and RIS models can be combined to provide a general description where proton binding and conformational equilibria are treated on equal footing, which is referred to as the SBRIS model [35]. In this case, one must specify the protonation state of each site and the conformational state of each bond, sometimes referred to as rotomicrostates [67]. Pair interactions between the sites will depend on the conformation of the bond in between, and the affinity constants of a site on the neighboring bonds. In the case of nearest-neighbor interactions, the model can be specified with the following 4×4 transfer matrix [35]

$$\mathbf{V}' = \begin{bmatrix} 1 & g & z_{tt} & gz_{tg} \\ 1 & gh & z_{tg} & ghz_{gg} \\ 1 & g & z_{tt}u_t & gz_{tg}u_t \\ 1 & gh & z_{tg}u_g & ghz_{gg}u_g \end{bmatrix} \tag{32}$$

where $z_{\alpha\beta} = K_{\alpha\beta}a_{\mathrm{H}}$ and $K_{\alpha\beta}$ is the binding constant of the site when the neighboring bonds are in the states α and β (α,β = t, g) and $\varepsilon_\alpha = -\log u_\alpha$.

This model can be again solved with transfer matrix techniques. However, we will not go into technical details, but again present some illustrative examples. For simplicity, we will assume that the binding constants do not depend on the conformations, and only discuss the effect of conformation on the site–site interactions.

Let us first discuss the situation without interactions between the bonds ($h = 1$). In this case, one finds the rather surprising result that the titration curve that follows from SBRIS model is exactly identical to the result of SB model with nearest-neighbor pair interactions eq. (17). The resulting pair interaction parameter is given by the thermally weighted mean between the corresponding interaction parameters for the two conformational states, namely

$$u = \frac{u_{\mathrm{t}} + gu_g}{1+g} \tag{33}$$

The situation is illustrated in Fig. 8A. In basic conditions, the chain is predominantly in the more favorable gauche state since no repulsive interactions are active. As the chain protonates, the repulsive interactions become more important and the chain minimizes those by switching to the trans state. The resulting binding isotherm lies in between the curves for the gauche and trans state, respectively.

The situation turns out to be more complicated in the presence of interactions between the bonds. However, the key result is that the overall binding isotherm can be still described with the SB model, albeit only approximately. One has to distinguish two different scenarios, namely the case of repulsive and attractive interactions between the bonds.

Let us first discuss the more common case of repulsive bond–bond interactions ($h < 1$). This situation is shown in Fig. 8B. In this case, the resulting titration curve still resembles the result from the nearest-neighbor pair interactions, but becomes asymmetric. With the SB model, an asymmetric titration curve can be obtained by introducing higher order interaction parameters, such as triplets and quadruplets. Nearest-neighbor triplet interactions involve three neighboring sites. When such higher order parameters are introduced the resulting titration curves can be described easily with the SB model. For example, this scenario is encountered for LPEI [28].

The case of attractive bond–bond interactions ($h > 1$) may lead to the behavior shown in Fig. 8C. In this case, the transition between the gauche and trans state is very sudden, and the titration curve crosses rapidly from the curve characterizing the gauche state to the corresponding curve for the trans state. This situation was studied with computer simulations in detail [36,37,49–51]. This transition resembles a first-order phase transition, even though the curves remain fully continuous. In this situation, long portions of the polyelectrolyte chain assume two different conformations [35,37,68,69]. While some authors suspect that these two conformations correspond to coil and helix states, others have proposed that they reflect the coiled and extended states in the pearl-necklace structure [37]. One important example of this situation is poly (methacrylic acid) where the hydrophobic methyl groups induce such attractive interactions [35,69].

Similar effects to conformational degrees of freedom are encountered due to different polymer tacticities. Tacticity of a polymer chain refers to the different spatial arrangement of the side groups along the chain. A well known example of molecules of different tacticity is poly (fumaric acid) (PFA) and poly(maleic acid) (PMA), see Fig. 1. While the molecular connectivity is the same in both molecules, the carboxylic groups are arranged in these two polyelectrolytes in different directions with respect to the main chain. Different tacticities can be incorporated in the SB description by introducing a sequence of different transfer matrices, each of which represents a different spatial arrangement of the side groups [61,70]. The polyelectrolytes discussed so far have been assumed to be of regular tacticity. Random tacticity has similar consequences as conformational degrees of freedom, but the randomness results in titration curves that are more gradual and more featureless than its counterparts with regular tacticity.

5. Examples

In the following, we shall illustrate the applicability of the ideas discussed with several weak polyelectrolytes. Let us first focus on polycarboxylic acids, see Fig. 1. The best known representative is poly (acrylic acid) (PAA). This molecule has an aliphatic backbone, and every second carbon is linked to a carboxylic acid group. While PAA is usually syndiotactic, the tacticity of the molecule does not influence the titration behavior of the molecule too strongly [21,22].

The charging behavior of PAA has been studied by numerous authors [21–25]. Fig. 9 shows the binding isotherms for different ionic strengths adjusted with CsCl background electrolyte [25]. The

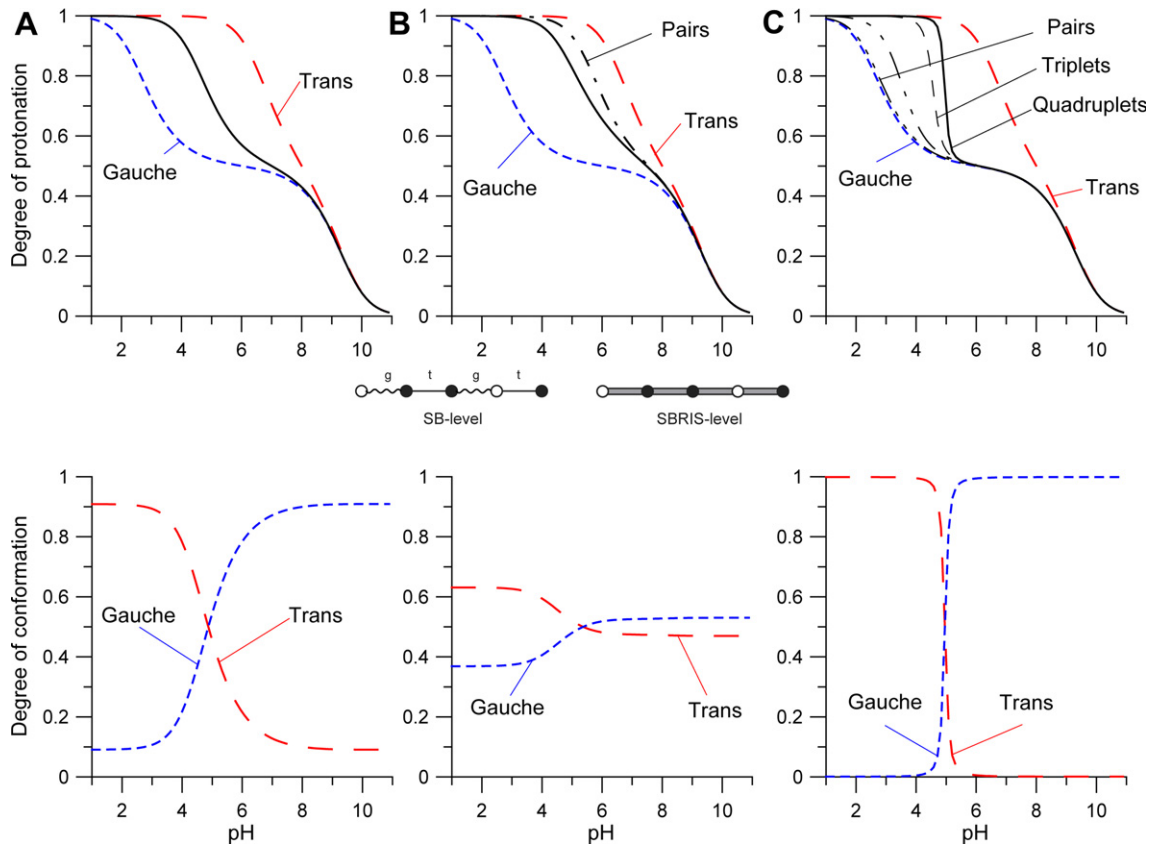

Fig. 8. Titration curves derived from SBRIS model with nearest-neighbor interactions and the corresponding contracted SB model. The binding constant $pK = 9$ independent of the conformation of the bonds, and pair interaction parameters $\varepsilon_g = 1$ and $\varepsilon_t = 3$. Degree of protonation (top) and conformational probabilities (bottom). Colour lines correspond to the titration curves of the all-gauche (short dashed, blue) and all-trans (long dashed, red) conformation. Predictions of the four-state SBRIS model (thick solid lines) are compared to the successive approximations on the contracted SB level including pair, triplet, and quadruplet interactions (thin lines). The schemes indicate the different levels of description. (A) No interactions ($h = 1$ and $g = 10$) where the contracted SB model with nearest-neighbor interactions is exact with $\varepsilon = 2$. (B) Repulsive interactions ($h = 0.3$ and $g = 10$) where the contracted SB description coincides at the triplet level with the exact result on the scale of the graph. (C) Attractive interactions ($h = 100$ and $g = 0.1$) where the contracted SB description does not even coincide with the exact result at the quadruplet level. (For interpretation of the references to colour in this figure legend, the reader is referred to the web version of this article).

representation as the effective ionization constant shows straight lines, which indicates the validity of the simple mean-field model. With increasing ionic strength, PAA becomes more acidic, in agreement with the DH model discussed above (see Fig. 7). However, the intrinsic binding constant also decreases with increasing ionic strength. The charging behavior of PAA depends weakly on the nature of the counterion [24,25]. Especially for smaller ions, some curvature in the pK_{eff} representation becomes apparent, which can be partly explained by non-linear nature of the PB model. Various authors conclude that PAA attains a more open

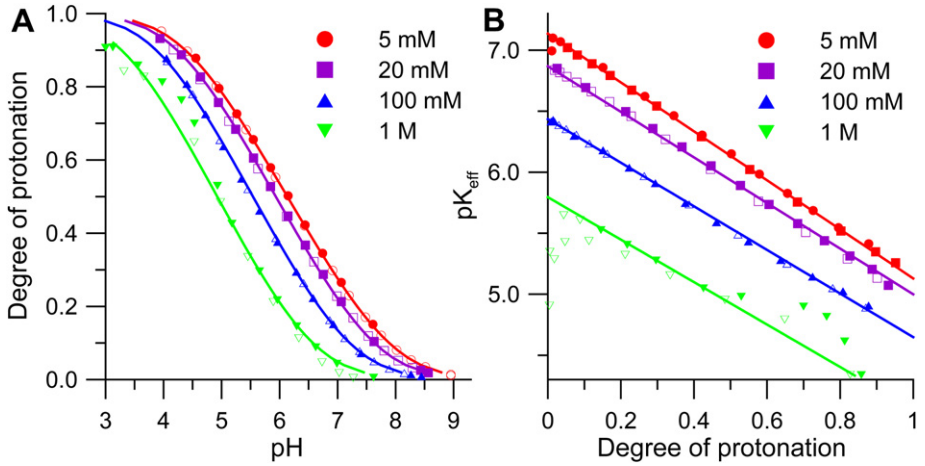

Fig. 9. Titration curves of poly(acrylic acid) (PAA) in CsCl electrolyte at 5 mM (red), 20 mM (purple), 100 mM (blue), and 1 M (green). The open and closed symbols indicate forward and backward titrations, respectively. (A) Degree of protonation θ as a function of pH and (B) effective binding constant pK_{eff} as a function of degree of protonation θ. (For interpretation of the references to colour in this figure legend, the reader is referred to the web version of this article).

conformation with increasing pH [23,35,38]. Very similar charging behavior was observed for hyaluronic acid, which is a polysaccharide with carboxylic groups [26].

Poly(methacrylic acid) leads to a charging curve with changes rapidly in a narrow pH region. This rapid change corresponds to a conformational transition of the polyelectrolyte, and is believed to be induced by the attractive hydrophobic interactions [23,35,69]. Similar behavior governed by a sudden conformational transition has been observed for poly(glutamic acid) [71,72], poly(3-thiophene acetic acid) [73,74], and other polycarboxylic acids [75,76].

Ionization behavior of PAA and poly(methacrylic acid) was also studied in the star-like architecture [48,77]. There was substantial interest in these branched structures recently [20,48,77–79]. In a star-polymer, linear chains emanate from a common center resembling the arms of a star-fish. Their number typically varies between 3 and 25. The ionization in star-like polyelectrolytes strongly resembles their linear analogs [48,77]. The reason for this behavior is again the short-range character of the site–site interactions. The ionizable sites interact principally with the nearest neighbors situated along the chain, while the interactions between the sites on different branches are screened and therefore much weaker. However, their presence leads to a minor increase the electrostatic repulsions between the sites and to a corresponding shift of the binding curve [20]. This effect has been observed experimentally for poly(acrylic acid) stars [48]. For a star with 21 arms, the shift of the midpoint of the binding curve is about 0.5 pH units at an ionic strength of about 0.01 M.

Let us now return to linear polycarboxylates, and discuss the titration curves of poly(fumaric acid) (PFA) and poly(maleic acid) (PMA) shown in Fig. 10. These polyelectrolytes have the same chemical structure, but they differ by their tacticity. Their maximum line charge density is twice as high as for PAA, and therefore the effects of interactions are more pronounced. In PMA, the carboxylic groups point predominantly in the same direction (i.e., isotactic chain), and this arrangement leads to the typical intermediate plateau in the titration curve [70]. This plateau signals the stability of the intermediate state with every second site protonated. The observed behavior can be described quantitatively by the nearest-neighbor pair SB model. One further observes an important influence on the nature of the monovalent counterions. The intermediate plateau becomes increasingly well developed with increasing size of these ions. The reasons for this behavior could be caused by the different distance of closest approach or by competition of the counterions with protons. This strong influence of the nature of the counterion is in substantial contrast to the weak dependence in the case of PAA. Poly(fumaric acid) (PFA) shows a more gradual titration curve. In PFA, the carboxylic groups point predominantly in opposite directions (i.e., syndiotactic chain).

Similar two-step titration curves were observed for linear polyamines, in particular, for poly(ethylene imine) (LPEI) [28] and poly(vinyl amine) (PVA) [13]. In these cases, however, the titration curves show an important asymmetry, which can be rationalized with triplet interactions.

Branched polyelectrolytes show more complicated charging behavior. The main features are that intermediate plateaus are not necessarily situated at half-protonation, and that broader and more featureless proton binding isotherms are the rule. This situation will be illustrated with branched polyamines, see Fig. 2.

Let us first address dendrimers as an example of hyperbranched polyamines. Two types of dendrimers with ionizable amine groups were described. The first is poly(propylene imine) (PPI) dendrimers [31] and the second poly(amido amine) (PAMAM) dendrimers [32,33]. Both dendrimers contain primary and tertiary amine groups only, albeit in different chemical environments. The charging behavior for both types of dendrimers is rather different. We will use the generation 2 dendrimer with 16 primary amine groups and 14 tertiary amine groups to illustrate the behavior. Higher generation dendrimers behave similarly.

In PPI dendrimers the amine groups are rather closely spaced and have similar chemical environment. For this reason, the mechanism suggested by the nearest-neighbor pair SB model discussed in Section 2 represents a reasonable approximation. The experimentally observed titration curves for PPI G2 dendrimers in KCl electrolyte are shown in Fig. 11A. As expected from the simple SB model, the protonation indeed proceeds in two steps with an intermediate plateau at $\theta = 2/3$. The binding isotherms also demonstrate that the dendrimers become more basic with increasing ionic strength. This behavior is in line with the DH model discussed above (see Fig. 7).

The titration curve can be quantified with the SB model. For the ionic strength of 0.1 M, the microscopic binding constants of the tertiary amines are 8.19, 7.99, 9.72 from the center to the outside, and of the outermost primary amine is 9.79. The nearest-neighbor pair interaction parameters are for the innermost pair 0.61, for the intermediate ones 1.05, and 1.57 for the outermost one. With these parameters, the observed titration curves can be reproduced quantitatively. With increasing ionic strength, one has an increase of the microscopic binding constants and a decrease of the interaction parameters.

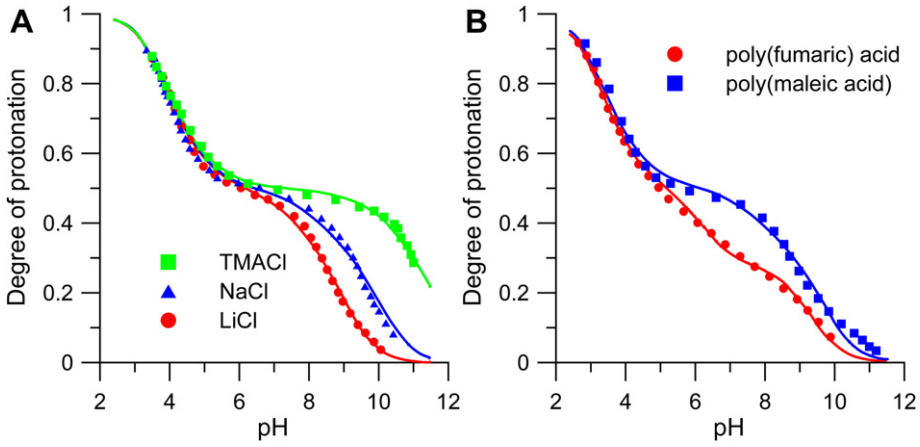

Fig. 10. Titration curves of highly charged polycarboxylates.(A) PMA (left) with 0.5 M tetramethylammonium chloride (TMACl, green), NaCl (blue), and LiCl (red). (B) Poly(maleic acid) (PMA, blue) and poly(fumaic acid) (PFA, red) at an ionic strength of 0.1 M NaCl. (For interpretation of the references to colour in this figure legend, the reader is referred to the web version of this article).

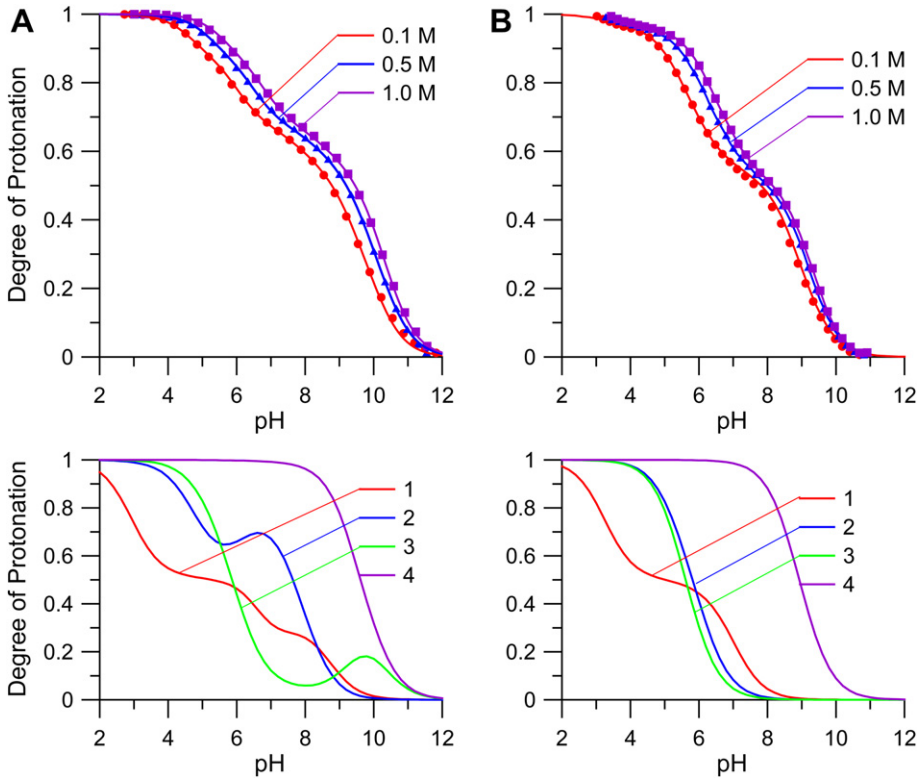

Fig. 11. Experimental binding isotherms of dendrimers of generation 2. Experimental binding isotherms different ionic strengths 0.1 M (red), 0.5 M (blue) and 1.0 M (purple, top row) and calculated site-specific titration curves at an ionic strength of 0.1 M (bottom row). First outer shell (1, purple), second outer shell (2, blue), third outer shell (3, green), and innermost fourth shell (4, red). (A) Polypropylene imine (PPI) and (B) poly(amido amine) (PAMAM). (For interpretation of the references to colour in this figure legend, the reader is referred to the web version of this article).

The protonation mechanism can be inferred from the site-specific titration curves. One observes that the outermost primary amine groups protonate at high pH, and the tertiary amine groups in the 3rd shell almost completely at somewhat lower pH. The protonation of these groups leads to the first intermediate plateau at $\theta = 2/3$. The remaining sites protonate at lower pH and lead to the second broad protonation step in the more acidic region.

In PAMAM dendrimers, the amine groups are rather far separated, and one therefore expects only weak interaction between these groups. On the other hand, the chemical environments of the primary and tertiary amine groups are rather different, thus suggesting that the primary groups are substantially more basic than the acidic ones. Since the number of primary and tertiary groups is the same, we expect an intermediate plateau at $\theta = 1/2$. The experimentally observed titration curves for PAMAM G2 dendrimers in 0.1 M KCl electrolyte are shown in Fig. 11B. Indeed, the protonation proceeds in two steps and the intermediate plateau lies at $\theta = 1/2$.

This scenario is confirmed by the calculation with the SB model. At an ionic strength of 0.1 M, the microscopic constants are for the tertiary amines 6.00 and 6.70 for the innermost one and 9.00 for

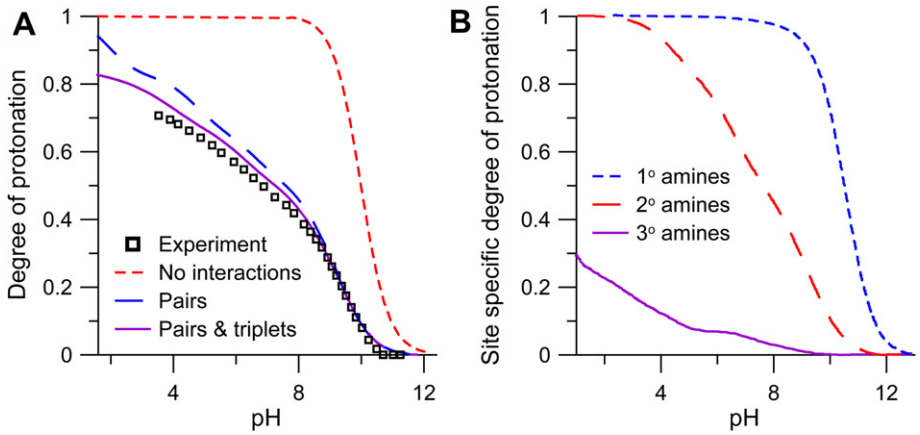

Fig. 12. Titration curves of branched poly(ethylene imine). (A) Experimental data points compared model results involving no interactions (short dashed, red), pair interactions only (log dashed, blue), and pair and triplet interactions (solid, purple). (B) Site-specific titration curves for the primary amines (short dashed, blue), secondary amines (long dashed, red) and tertiary amines (solid, purple) obtained from Monte Carlo simulations are shown in the left graph. (For interpretation of the references to colour in this figure legend, the reader is referred to the web version of this article).

the primary ones. The pair interaction parameters are 2.85 for the innermost pair, and 0.15 for the other bonds. In addition, there is a nearest-neighbor pair interaction between the primary amines of 0.14. With these parameters, the SB model explains the experimental titration data quantitatively. The microscopic constants increase with increasing ionic strength. The pair interaction between the primary amines decreases with increasing ionic strength, while the other interaction parameters vary only weakly, and can be assumed to be constant to good approximation.

The protonation mechanism can be inferred from the site-specific titration curves. Again, all primary amines protonate in the basic region. Due to weak interactions, the tertiary sites protonate almost independently, and they all protonate simultaneously in more acidic conditions. The only exceptions are the two innermost sites, which interact strongly and therefore protonate in a step wise fashion. However, their contribution is negligible for larger dendrimers.

Recently, there was substantial interest in the conformational transformation of dendrimers and their eventually swelling with increasing charge [52–54,80,81]. While earlier theoretical work suggested substantial swelling with increasing charge, neutron scattering experiments indicate that only marginal swelling occurs [54,81]. This observation was later reconciled with detailed computer simulations studies [53].

Finally, let us discuss branched poly(ethylene imine) (BPEI), see Fig. 2 [30,34,82,83]. BPEI is a randomly branched molecule containing primary, secondary, and tertiary amines in a ratio of about 1:2:1. The experimental titration data of BPEI in 0.5 M NaCl are shown in Fig. 12A [83]. The degree of protonation increases rapidly in the basic region until about half of the sites are protonated, and then rises much more slowly. In fact, BPEI does never completely protonate in the accessible pH region.

The nearest-neighbor pair interaction SB model for BPEI can be devised in analogy to the discussion above. A common set of parameters was obtained for polyamines based on small molecules [30]. The microscopic affinity constants are 9.64, 8.59, and 7.50 for the primary, secondary, and tertiary amines. The nearest-neighbor pair interaction parameter is $\varepsilon = 1.85$. For a quantitative description, one must further introduce a next nearest-neighbor pair interaction parameter 0.27 acting between amine groups neighboring a tertiary amine, and a nearest-neighbor interaction triplet interaction parameter of 0.27. Based on these parameters, the titration curve is obtained by Monte Carlo simulations. Fig. 12 also illustrates the effects of the higher order interaction parameters. The model invoking nearest-neighbor pair interactions only captures the overall behavior, but overestimates the degree of protonation at low pH.

These curves clearly illustrate the protonation mechanism of BPEI. At high pH, all primary amines do protonate without invoking any interactions. Almost simultaneously, about half of the secondary amines protonate, which leads to the first relatively steep protonation step near pH 8–10. At lower pH, the secondary amines protonate further together with the tertiary ones. Around pH 4 most of the secondary amines are protonated, but only a fraction of the tertiary ones. The reason why the tertiary amines protonate only at very low pH is related to the fact that they are surrounded with protonated sites, which makes them very acidic with a microscopic constant given by $pK - 3\varepsilon = 1.95$. For this reason, tertiary amine groups start to protonate appreciably only in very acidic conditions.

6. Conclusion

The present article summarizes our current understanding of ionization processes of weak polyelectrolytes. The aim was to present the general concepts of the site binding models, which are able to account for many experimental features of linear and branched polyelectrolytes. In particular, they explain the intermediate plateaus that are often observed for highly charged polyelectrolytes as stable microscopic states where the charged sites are arranged in an alternative fashion. These states occur due to the short-ranged character of the site–site interactions, which is probably related to the low dielectric constant within an aliphatic chain. Conformational equilibria equally affect the ionization process and they may lead to higher order interactions or transition phenomena resembling first-order phase transitions. Ionization of polyelectrolytes is equally affected by the nature of the counterions present. The latter phenomena are still poorly understood, and their clarification requires further investigation.

Acknowledgement

This research was supported by the University of Geneva, Technical University of Delft, Swiss National Science Foundation, and the COST Action D43.

References

[1] Hiemenz PC. Polymer chemistry. New York: Marcel Dekker; 1984.
[2] Elias HG. Macromolecules. New York: John Wiley; 2009.
[3] Borkovec M, Jonsson B, Koper GJM. Colloid Surf Sci 2001;16:99–339.
[4] Ullner M. In: Tripathy SK, Kumar J, Nalwa HS, editors. Handbook of polyelectrolytes and their applications, vol. 3. New York: American Scientific Publishers; 2002.
[5] Holm C, Joanny JF, Kremer K, Netz RR, Reineker P, Seidel C, et al. Adv Polym Sci 2004;166:67–111.
[6] Borkovec M, Koper GJM, Piguet C. Curr Opin Colloid Interf Sci 2006;11:280–9.
[7] Borkovec M, Koper GJM. J Phys Chem 1994;98:6038–45.
[8] Mernissi-Arifi K, Schmitt L, Schlewer G, Spiess B. Anal Chem 1995;67:2567–74.
[9] Borkovec M, Koper GJM. Anal Chem 2000;72:3272–9.
[10] Noszal B, Szakacs Z. J Phys Chem B 2003;107:5074–80.
[11] Frassineti C, Alderighi L, Gans P, Sabatini A, Vacca A, Ghelli S. Anal Bioanal Chem 2003;376:1041–52.
[12] Steiner RF. J Chem Phys 1954;22:1458–9.
[13] Katchalsky A, Mazur J, Spitnik P. J Polym Sci 1957;23:513–32.
[14] Marcus RA. J Phys Chem 1954;58:621–3.
[15] Ising E. Z Phys 1925;31:253–8.
[16] Ercolani G. J Am Chem Soc 2003;125:16097–103.
[17] Acerenza L, Mizraji E. Biochim Biophys Acta 1997;1339:155–66.
[18] Perlmutter-Hayman B. Acc Chem Res 1986;19:90–6.
[19] Raphael E, Joanny JF. Europhys Lett 1990;13:623–8.
[20] Klein Wolterink J, van Male J, Cohen Stuart MA, Koopal LK, Zhulina EB, Borisov OV. Macromolecules 2002;35:9176–90.
[21] Nagasawa M, Murase T, Kondo K. J Phys Chem 1965;69:4005–12.
[22] Kawaguchi Y, Nagasawa M. J Phys Chem 1969;73:4382–4.
[23] Sakurai M, Imai T, Yamashita F, Nakamura K, Komatsu T, Nakagawa T. Polym J 1993;25:1247–55.
[24] De Stefano C, Gianguzza A, Piazzese D, Sammartano S. React Funct Polym 2003;55:9–20.
[25] Sadeghpour A, Vaccaro A, Rentsch S, Borkovec M. Polymer 2009;50:3950–4.
[26] Cleland RL, Wang JL, Detweiler DM. Macromolecules 1982;15:386–95.
[27] Kitano T, Kawaguchi S, Ito K, Minakata A. Macromolecules 1987;20:1598–606.
[28] Smits RG, Koper GJM, Mandel M. J Phys Chem 1993;97:5745–51.
[29] Koper GJM, van Duijvenbode RC, Stam DDPW, Steuerle U, Borkovec M. Macromolecules 2003;36:2500–7.
[30] Borkovec M, Koper GJM. Macromolecules 1997;30:2151–8.
[31] van Duijvenbode RC, Borkovec M, Koper GJM. Polymer 1998;39:2657–64.
[32] Cakara D, Kleimann J, Borkovec M. Macromolecules 2003;36:4201–7.
[33] Niu YH, Sun L, Crooks RA. Macromolecules 2003;36:5725–31.
[34] Griffiths PC, Paul A, Stilbs P, Petterson E. Macromolecules 2005;38:3539–42.
[35] Garces JL, Koper GJM, Borkovec M. J Phys Chem 2006;110:10937–50.
[36] Uyaver S, Seidel C. Europhys Lett 2003;64:536–42.
[37] Uyaver S, Seidel C. J Phys Chem B 2004;108:18804–14.
[38] Ullner M, Jonsson B. Macromolecules 1996;29:6645–55.
[39] Ullner M, Woodward CE. Macromolecules 2000;33:7144–56.
[40] Borkovec M, Daicic J, Koper GJM. Proc Natl Acad Sci U S A 1997;94:3499–503.
[41] Borkovec M, Daicic J, Koper GJM. Physica A 2001;298:1–23.
[42] Panagiotopoulos AZ. J Phys Condens Matter 2009;21.
[43] Burak Y, Netz RR. J Phys Chem B 2004;108:4840–9.
[44] Netz RR. J Phys Condens Matter 2003;15:S239–44.
[45] Ziebarth JD, Wang YM. Biomacromolecules 2010;11:29–38.
[46] Zito T, Seidel C. Eur Phys J E 2002;8:339–46.
[47] Castelnovo M, Sens P, Joanny JF. Eur Phys J E 2000;1:115–25.

[48] Plamper FA, Becker H, Lanzendorfer M, Patel M, Wittemann A, Ballauff M, et al. Macromol Chem Phys 2005;206:1813–25.
[49] Ulrich S, Laguecir A, Stoll S. J Chem Phys 2005;122:094911.
[50] Yamaguchi T, Kiuchi T, Matsuoka T, Koda S. Bull Chem Soc Jpn 2005;78:2098–104.
[51] Uyaver S, Seidel C. Macromolecules 2009;42:1352–61.
[52] Ballauff M, Likos CN. Angew Chem Int Ed 2004;43:2998–3020.
[53] Liu Y, Bryantsev VS, Diallo MS, Goddard WA. J Am Chem Soc 2009;131:2798–9.
[54] Porcar L, Liu Y, Verduzco R, Hong KL, Butler PD, Magid LJ, et al. J Phys Chem B 2008;112:14772–8.
[55] Koper GJM, Borkovec M. J Chem Phys 1996;104:4204–13.
[56] Borkovec M, Rusch U, Cernik M, Koper GJM, Westall JC. Colloids Surf A 1996;107:285–96.
[57] Cernik M, Borkovec M, Westall JC. Environ Sci Technol 1995;29:413–25.
[58] Avena MJ, Koopal LK, van Riemsdijk WH. J Colloid Interf Sci 1999;217:37–48.
[59] Kinniburgh DG, van Riemsdijk WH, Koopal LK, Borkovec M, Benedetti MF, Avena MJ. Colloids Surf A 1999;151:147–66.
[60] Wyman J, Gill SJ. Binding and linkage. Mill Valley: University Science Books; 1990.
[61] Flory PJ. Statistical mechanics of chain molecules. New York: Interscience; 1969.
[62] van Duijvenbode RC, Rajanayagam A, Koper GJM, Baars MWPL, de Waal BFM, Meijer EW, et al. Macromolecules 2000;33:46–52.
[63] Ritchie JD, Perdue EM. Geochim Cosmochim Acta 2003;67:85–96.
[64] Reed CE, Reed WF. J Chem Phys 1992;96:1609–20.
[65] Hill TL. Arch Biochem Biophys 1955;57:229–34.
[66] Penfold R, Jonsson B, Nordholm S. J Chem Phys 1993;99:497–514.
[67] Kraszni M, Szakacs Z, Noszal B. Anal Bioanal Chem 2004;378:1449–63.
[68] Khokhlov AR, Kramarenko EY. Macromolecules 1996;29:681–5.
[69] Cesaro A, Paoletti S, Guidugli S, Benegas JC. Biophys Chem 1991;39:9–16.
[70] de Groot J, Koper GJM, Borkovec M, de Bleijser J. Macromolecules 1998;31:4182–8.
[71] Appel P, Yang JT. Biochemistry 1965;4:1244.
[72] Olander DS, Holtzer A. J Am Chem Soc 1968;90:4549–60.
[73] Kim BS, Chen L, Gong JP, Osada Y. Macromolecules 1999;32:3964–9.
[74] Vallat P, Catala JM, Rawiso M, Schosseler F. EPL 2008;82:28009.
[75] Dubin P, Strauss UP. J Phys Chem 1973;77:1427–31.
[76] Villiers C, Braud C. New J Chem 1978;2:33–8.
[77] He E, Yue CY, Tam KC. Langmuir 2009;25:4892–9.
[78] Jusufi A, Likos CN. Rev Mod Phys 2009;81:1753–72.
[79] He E, Ravi P, Tam KC. Langmuir 2007;23:2382–8.
[80] Welch P, Muthukumar M. Macromolecules 1998;31:5892–7.
[81] Nisato G, Ivkov R, Amis EJ. Macromolecules 2000;33:4172–6.
[82] Horn D. In: Goethals EJ, editor. Polymeric amines and ammonium salts. Oxford, New York: Pergamon Press; 1980. p. 333–55.
[83] Balif JB, Lerf C, Schlapfer CW. 1994;48: 336–42.

Dr. Ger J.M. Koper is Associate Professor at the Chemical Engineering Department of the Delft University of Technology. He became Electronics Engineer in 1975 and worked as such in the Department of Histochemistry and Cytochemistry of the Leiden University from 1976 to 1985. He received his PhD degree from Leiden University in 1990 on Aging in Spin Glasses with Prof. Dr. H.J. Hilhorst from the Lorentz Institute for Theoretical Physics as supervisor. From 1990 until 2000 he was Senior Lecturer at the Physical and Macromolecular Chemistry group with Prof. Dr. D. Bedeaux and Prof. Dr. J.C. Leyte. His research field is Physical Chemistry with emphasis on Colloid and Interface Science. He co-authored more than 125 publications in referred journals.

Professor Michal Borkovec obtained his PhD in Physical Chemistry from Columbia University, New York, in 1986, and was working thereafter as a Lecturer at the Swiss Federal Institute of Technology. In 1998 he became Associate Professor level at Clarkson University, and was appointed in 2001 as full professor in chemistry at the University of Geneva. He co-authored more than 170 publications in referred journals, his work was cited more than 8000 times, and he was honored for his work by the Rafael-Eduard-Liesegang-Prize from the German Colloid Society in 2001, then by the title of Invited Lecturer from the Otto Warburg Foundation of the University of Bayreuth in 2006. Since 2009, he is member of the Swiss National Research Council.